

# Preparation and Property of Modified Micro-arc Oxidation Coating Using Al<sub>2</sub>O<sub>3</sub> Particles on Ti6Al4V

Li Hong<sup>1</sup>, Song Zhihui<sup>1,2</sup>, Tang Peng<sup>1</sup>

<sup>1</sup> Key Lab of Guangdong for Modern Surface Engineering Technology, National Engineering Laboratory for Modern Materials Surface Engineering Technology, Guangdong Institute of New Materials, Guangzhou 510650, China; <sup>2</sup> Guangdong University of Technology, Guangzhou 510006, China

**Abstract:** Micro-arc oxidation is a new surface treatment method, but the structure of the micro-arc oxidation coating is restricted by the electrolyte composition. The micro-arc oxidation coating on Ti6Al4V alloy was modified by adding micro-Al<sub>2</sub>O<sub>3</sub> particles to a sodium phosphate solution. The coating structure and phase were characterized by scanning electron microscopy and X-ray diffraction, and the oxidation resistance and thermal shock properties of the coating were investigated. Results show that the modified coating is denser than the original coating, which is composed of Al<sub>2</sub>TiO<sub>5</sub> and TiO<sub>2</sub>. The oxidation resistance and thermal shock property of the coating are improved with addition of Al<sub>2</sub>O<sub>3</sub> particles in the electrolyte compared to those of the samples prepared without particles added in the electrolyte. Moving Al<sub>2</sub>O<sub>3</sub> particles are adsorbed on the coating surface and penetrate through it. As a result, the phase structure and properties of the original coating are modified.

**Key words:** Ti6Al4V; micro-arc oxidation; Al<sub>2</sub>O<sub>3</sub> particle; oxidation resistance; thermal shock property

Titanium alloys are widely used in the aerospace and biomedical industries for their low density, high relative strength, and good corrosion resistance. However, these alloys exhibit poor tribological behavior and anti-oxidation resistance at high temperatures. Micro-arc oxidation (MAO) is a new surface modification technique that has been widely investigated in recent years and employed to produce different kinds of coatings on Ti alloys with improved properties<sup>[1-4]</sup>. Basically, the composition of the MAO coating depends on the substrate (Mg, Al, or Ti alloy) and the electrolyte. For example, TiO<sub>2</sub>, Al<sub>2</sub>O<sub>3</sub>, and SiO<sub>2</sub> coatings are generally prepared in phosphate<sup>[5]</sup>, aluminate<sup>[6]</sup>, and silicate<sup>[5]</sup> solutions, respectively. Other composite coatings prepared in mixed solutions<sup>[7]</sup> are used on titanium alloys. The porous structure of the MAO coating is generated due to the micro-arc property of the approach<sup>[8]</sup>. The in-situ growth behavior of the MAO coating underlies its good adhesion to the substrate<sup>[9]</sup>. Favorable thermal resistance of

the MAO coating has also been reported<sup>[10, 11]</sup>. The MAO coating prepared in Na<sub>2</sub>SiO<sub>3</sub>-Na<sub>2</sub>CO<sub>3</sub>-NaOH solution on Ti6Al4V exhibits good anti-oxidation properties at 500 °C for 200 h<sup>[10]</sup>. The coating prepared in sodium phosphate with Co(CH<sub>3</sub>COO)<sub>2</sub> addition on Ti6Al4V exhibits thermal shock resistance at 500 °C for 40 cycles<sup>[11]</sup>. Also, the functional coatings prepared on Ti alloys using MAO technology have attracted attention. The black coating, first produced in the 1980s by the original anode oxidation technique or the cathode plasma oxidation method, is obtained in mixed electrolyte<sup>[12]</sup>. Overall, the coating properties are mostly dependent on the electrolyte employed.

In this study, a MAO coating much denser than usual was prepared on Ti6Al4V alloy by adding Al<sub>2</sub>O<sub>3</sub> particles to sodium phosphate solution. The effects of this coating on anti-oxidation at 700 °C and thermal shock at 850 °C were studied.

## 1 Experiment

Received date: March 02, 2019

Foundation item: 2017GDAS' Special Project of Science and Technology Development (2017GDASCX-0844, 2017GDASCX-0111); 2017GDAS' Academician Fund (2017GDASCX-0202)

Corresponding author: Li Hong, Ph. D., Key Lab of Guangdong for Modern Surface Engineering Technology, National Engineering Laboratory for Modern Materials Surface Engineering Technology, Guangdong Institute of New Materials, Guangzhou 510650, P. R. China, Tel: 0086-20-37238071, E-mail: leehongaaron@163.com

### 1.1 Coating preparation

The substrate material used in this investigation was Ti6Al4V titanium alloy (Baoji Dingding Titanium Products Co., Ltd), with a chemical composition of 6.3 wt% Al, 4.2 wt% V, 0.15 wt% O, 0.11 wt% Fe, 0.03 wt% C, 0.02 wt% N, 0.001 wt% H, and balance Ti. Specimens with a size of 20 mm×15 mm×2 mm were ground using 60<sup>#</sup>, 120<sup>#</sup>, 400<sup>#</sup>, 600<sup>#</sup>, 1000<sup>#</sup>, and 1500<sup>#</sup> grit silicon carbide papers. The specimens were then cleaned using distilled water and acetone and subsequently air dried. For MAO treatment, a unipolar pulse power supply was employed, and the Ti6Al4V plate was used as the anode electrode. A graphite plate was used as the cathode in the electrolytic cell. The electrolyte was composed of an aqueous solution containing 0.3 mol/L sodium phosphate solution (Sinopharm Chemical Reagent Co., Ltd) and 6 g/L Al<sub>2</sub>O<sub>3</sub> particles (Hefei Zhonghang Nanometer Technology Development Co., Ltd) dispersed by a magnetic stirrer, while the container was filled with 2 L deionized water. During MAO treatment, the temperature of the electrolyte was maintained below 45 °C. The applied parameters are shown in Table 1. MAO coatings prepared in sodium phosphate solution without Al<sub>2</sub>O<sub>3</sub> particles were used as a basis for comparison. After treatment, the obtained samples were washed with distilled water and dried at room temperature. The samples were then designed as TMPAl (Al<sub>2</sub>O<sub>3</sub> particles within electrolyte) and TMP (without Al<sub>2</sub>O<sub>3</sub> particles in the electrolyte).

### 1.2 Characterization of the coating

The size of Al<sub>2</sub>O<sub>3</sub> particles was measured by a laser diffraction particle size analyzer (LMS-30). The current was noted and the growth kinetics curves were plotted. The roughness of the samples was measured by a roughness gauge (TR200, Time Group Inc., China). The phase component of the samples was analyzed by X-ray diffraction (XRD; Cu K $\alpha$  radiation, DMAX-RB, scanning in the range of 2 $\theta$  = 10°~80°, 0.02°/step, 40 kV, 150 mA). Scanning electron microscopy (SEM; FEI Quanta250 Environmental scanning electron microscope) was employed to observe the coating morphology.

### 1.3 Properties of the coating

A thermal high-temperature cyclic oxidation test was performed in a kryptol heater furnace at 700 °C in air for 100 h. A ceramic crucible was used to hold the sample and pre-heated to a constant mass. The Ti6Al4V substrate and the coating sample were previously weighted, and then oxidized at 700 °C for 10 h. All of the specimens were then brought out, cooled naturally in air to room temperature, and then weighted again. Afterward, the samples were returned to the

furnace for the next heating at 700 °C for 10 h. Every 10 h of heating at 700 °C means one thermal cycle. The test was performed for 10 thermal cycles, and the size of each sample was measured before the thermal cycle oxidation test. The mass gain of each sample is obtained by dividing the surface area by the mass gain of each sample. And the kinetic curve of each mass variant per unit area versus time was plotted.

A thermal shock test was conducted to evaluate the thermal shock property of the coating and the bond strength between the coating and substrate. The coated sample was placed inside a furnace at 850 °C for 10 min. The specimen was then immediately removed, immersed in cool water, and returned to the furnace for the subsequent cycle. The thermal shock test was repeated for 30 cycles. The surface morphology and thermal-control property of the coatings were observed.

## 2 Results and Discussion

### 2.1 Particle size distribution of Al<sub>2</sub>O<sub>3</sub>

Fig.1 shows the particle size distribution of Al<sub>2</sub>O<sub>3</sub> particles, and vol% means the percentage of particles per size. The Al<sub>2</sub>O<sub>3</sub> particles measure about 1  $\mu$ m and ranges between 0.3 and 3.6  $\mu$ m. The added Al<sub>2</sub>O<sub>3</sub> particles were dispersed by a magnetic stirring apparatus located at the bottom of the container.

### 2.2 Current-time response

The current-time response of the TMP and TMPAl coatings are shown in Fig.2, and the voltage is 500 V. Three main regions [13] can be identified in both curves. The current-time curves initially decline linearly, gradually dip, and then stabilize. By comparing the two curves, we noted that the current in the coat-forming process of TMPAl is lower than that of TMP and stabilizes at a very low value. The temperature of micro-arc on the substrate can reach 4000 K, causing partial melting [14]. So the moving Al<sub>2</sub>O<sub>3</sub> particles are adsorbed onto the coating surface and penetrate it. The Al<sub>2</sub>O<sub>3</sub> particles melt and recrystallize together, thereby increasing volume. Many micro-arc pores are filled, and a denser coating forms which causes an increases in resistance, and at the same time, the electrolyte resistance in-

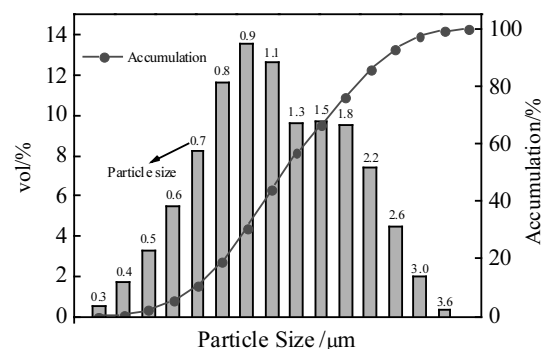


Fig.1 Particle size distribution of Al<sub>2</sub>O<sub>3</sub>

Table 1 Parameters for MAO coating preparation

Voltage/V	Pulse frequency/Hz	Duty ratio/%	Time/min
500	2000	60	10

creases due to the addition of  $\text{Al}_2\text{O}_3$  particles, resulting in a decrease in current density during micro-arc oxidation process.

### 2.3 Microcosmic surface morphologies of the coatings

The microscopic surface morphologies of the coatings are depicted in Fig.3. Many micron-sized pores <sup>[15, 16]</sup> generated by the micro-arc reaction are observed on the surface of TMP (Fig.3a), whereas a few pores exist on the TMPAl surface (Fig.3b). The micro-arc occurs at applied voltages above the breakdown voltage of the gas layer enshrining the substrate <sup>[17]</sup>. The generation of a micro-arc depends on the applied voltage and the gas layer formed by the anodic oxidation reaction. The moving  $\text{Al}_2\text{O}_3$  particles constantly affect the gas layer; hence, these particles do not produce sufficient plasma to create a micro-arc. Pores are fewer and smaller on the surface of the TMPAl coating than on the TMP coating. Meanwhile, the coating density and conductivity affect the process of anodic oxidation. The density of TMPAl is better than that of TMP. Throughout the experiment, the current of TMPAl is lower than that of TMP. Hence, less micro-arc is generated on the surface of TMPAl, leading to fewer pores compared to TMP.

The micro morphology of the coating with the addition of  $\text{Al}_2\text{O}_3$  particles is shown in Fig.3b, and few micro-particles appear on the coating surface. Two key points on the surface of the TMPAl coating are marked for energy dispersive spectroscopy (EDS) analysis, one in uniform area and the other in a particle position. Table 2 shows the EDS results of point A and B. A dense area was noted around point A, mainly consisting of O, Al, Ti, and a small amount of P. P originates from the electrolyte after firing at high temperatures caused by micro-arc <sup>[9]</sup>. Al mostly comes from the added  $\text{Al}_2\text{O}_3$  particles in the electrolyte. O is contributed by the  $\text{Al}_2\text{O}_3$  particles and the oxidation of Ti. The determined levels of O, Al, and Ti conform to the composition of  $\text{Al}_2\text{O}_3$  and  $\text{TiO}_2$ . Hence, the composition of point A resembles  $\text{Al}_2\text{O}_3$ ,  $\text{TiO}_2$ , and the combination of  $\text{Al}_2\text{O}_3$  and  $\text{TiO}_2$ .

Point B corresponds to added  $\text{Al}_2\text{O}_3$  particles, which are composed of O, Al, Ti, and some P. Compared with point A, the content of Ti in point B is apparently low. In contrast,

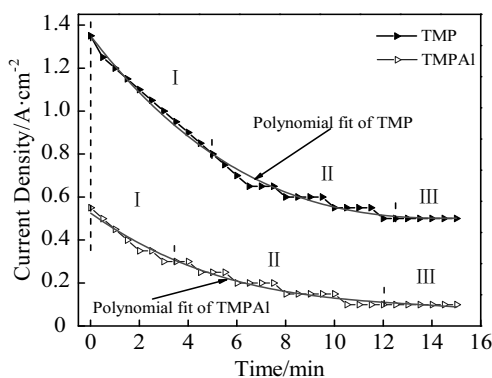


Fig.2 Current-time response of TMP and TMPAl coatings

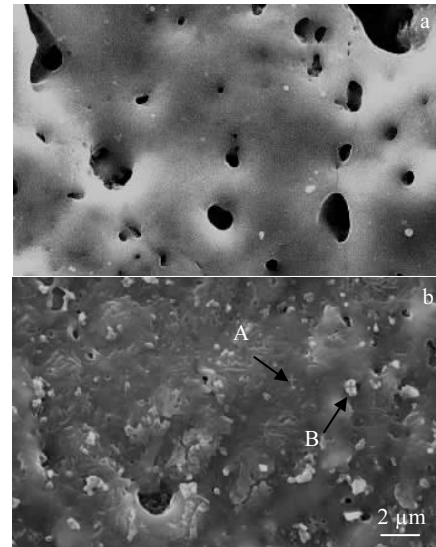


Fig.3 SEM images of surface morphology of TMP (a) and TMPAl (b) coatings

the relative amounts of O, Al and Ti also resemble the composition of  $\text{Al}_2\text{O}_3$  and  $\text{TiO}_2$ . And, the main composition is  $\text{Al}_2\text{O}_3$ , so the point B can be concluded to the  $\text{Al}_2\text{O}_3$  particle.

### 2.4 Coating phases

Fig.4 shows the XRD patterns of TMP, TMPAl, and their oxidized counterparts. The main phase of the coating prepared in sodium phosphate solution without  $\text{Al}_2\text{O}_3$  particles corresponds to metastable anatase  $\text{TiO}_2$  at low temperature, thermodynamically stable rutile  $\text{TiO}_2$  at almost all temperatures, and Ti. These results are similar to those previously reported <sup>[9]</sup>. During the MAO process, the anode Ti6Al4V is oxidized to form anatase  $\text{TiO}_2$ , part of which transforms to rutile  $\text{TiO}_2$  at high temperatures caused by the micro-arc discharge. Furthermore, the discharge channel promotes the migration of Ti from the substrate to the coating. With increasing the coating thickness, the previously formed coating becomes calcined and sputtered, allowing the transfer of some Ti from the substrate to the coating. After oxidation at 700 °C for 100 h, Ti is oxidized to titanium dioxide. As the transformation temperature of anatase  $\text{TiO}_2$  to rutile  $\text{TiO}_2$  reaches 600 °C, much more rutile  $\text{TiO}_2$  appears.

Table 2 Elemental composition of TMPAl at point A and B in Fig.3b (at%)

Point	Element			
	O	Al	Ti	P
A	62.55	18.73	17.82	0.90
B	58.94	34.78	5.50	0.78

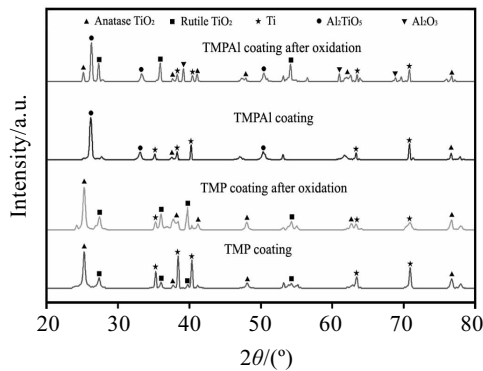
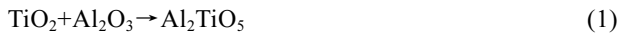


Fig.4 XRD patterns of TMP and TMPAI coatings before and after oxidation at 700 °C for 100 h

The main phases of the coating prepared in sodium phosphate solution with  $\text{Al}_2\text{O}_3$  particles are  $\text{Al}_2\text{TiO}_5$ , Ti, and some anatase  $\text{TiO}_2$ . The reported temperature of the following reaction<sup>[18]</sup> is 1553 K. In the formation process, the  $\text{Al}_2\text{O}_3$  particle is absorbed into the melting  $\text{TiO}_2$  to form  $\text{Al}_2\text{TiO}_5$ . The presence of Ti is caused by the permeation in high-voltage condition and sputtering by the micro-arc. Similar to TMP, Ti in the TMPAI coating becomes oxidized into anatase  $\text{TiO}_2$  and rutile  $\text{TiO}_2$ . Moreover,  $\text{Al}_2\text{TiO}_5$  is partially decomposed into  $\text{TiO}_2$  and  $\text{Al}_2\text{O}_3$ , as shown in the reaction below:



## 2.5 High-temperature oxidation of samples

Fig.5 shows the curves of mass gain for the coating samples and substrate versus time under isothermal cyclic oxidation at 700 °C for 100 h. After oxidation, the color of Ti6Al4V drastically changes; the brown oxide coating is generated and peels off massively with time. The TMP transforms from light grey to light yellow, whereas the TMPAI changes slightly. No spalling pieces are found on both TMP and TMPAI after oxidation. Notably, the oxidation kinetics curve of Ti6Al4V follows parabolic kinetics before 30 h because the oxide coating does not spall from the substrate. Then, the curve follows linear kinetics, as the oxide coating begins to spall gradually. The surface SEM morphologies of TMP and TMPAI after oxidation are shown in Fig.6. TMP samples form a certain amount of cracks, but no obvious cracks are observed in TMPAI samples, and there is no piece spalling off from the substrate. The mass gains of TMP and TMPAI are 0.78 and 0.60  $\text{mg}/\text{cm}^2$ , respectively, illustrating that the coating samples of TMP and TMPAI can both provide good oxidation resistance for Ti6Al4V at 700 °C for 100 h. The mass gains of TMP and TMPAI mainly caused by the oxidation of Ti are observed in the coatings. The content of Ti in TMP is substantially greater than that in TMPAI, as shown in XRD patterns (Fig.4). Meanwhile, the presence of cracks in TMP causes more oxygen to enter the interior of the coating to react

with the titanium in the coating when oxidized at high temperatures, so TMP exhibits greater oxidation gain than TMPAI. Hence, the mass gain of TMP is much higher than that of TMPAI. Compared with the substrate, TMP and TMPAI have a 10% oxidation mass gain than the substrate, showing better oxidation resistance. The good oxidation resistance properties of TMP and TMPAI can be attributed to the phase and coating structure. The main phases of TMP and TMPAI are  $\text{TiO}_2$ ,  $\text{Al}_2\text{O}_3$ , and  $\text{Al}_2\text{TiO}_5$  with low oxygen diffusion coefficients. The structure of TMP contains both porous and dense layers. Although many pores exist in the porous layer, these pores are insufficient, and thus no channels are available for oxygen to reach the substrate. While the appearance of cracks accelerates the diffusion of external oxygen into the inside, and more Ti in the coating is oxidized, so oxidation gain increases. In contrast, TMPAI possess fewer pores, and consequently, oxygen is much more difficult to pass through the TMPAI coating.

According to the Wagner's theory of oxidation<sup>[19]</sup>, oxidation mass gain and oxidation time can be expressed by the following relationship:

$$\Delta W^n = k_p \cdot t \quad (2)$$

where  $n$  is reaction index,  $k_p$  is reaction constant (function of temperature),  $\Delta W$  is mass gain, and  $t$  is oxidation time. The method of linear regression was adopted to fit the curve and to calculate the reaction index and reaction constant. The fitting equation is shown in Table 3, in which  $D$  is fitting error, and the smaller the  $D$  value, the closer the fitting curve to the true value. Generally, when the  $D$  value is less than  $10^{-2}$ , the fitting equation is useful.

From the value of  $n$  in Table 3, continuous oxidation is used to describe the oxidation of the Ti6Al4V substrate as the oxidation film spalls off with time. Linear oxidation occurs on the TMP coating, whereas parabolic oxidation takes place on the TMPAI coating. The extended oxidation from 100 h to 300 h is plotted in Fig.5 according to the oxidation kinetic equations, and the TMPAI coating can provide better anti-oxidation protection for Ti6Al4V than TMP in the long time.

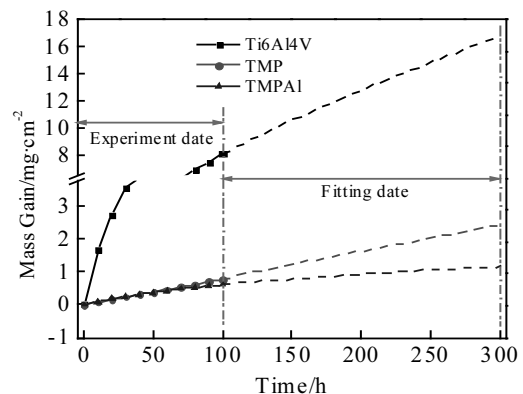


Fig.5 Oxidation kinetics curves of the samples under oxidation at 700 °C for 100 h and fitting date from 100 h to 300 h

## 2.6 Thermal shock property of coatings

The surface macro-photographs of the coating samples after 30 times of thermal shock testing at 850 °C are exhibited in Fig.7. A large area of TMP is peeled off, whereas some scattered oxidation points are displayed on the surface of TMPAl. These points indicate that the thermal shock resistance of the MAO coating prepared in sodium phosphate solution can be improved by the addition of appropriate  $\text{Al}_2\text{O}_3$  particles in the electrolyte. The thermal shock property is used to describe the anti-thermal shock property of some coatings and the adhesion between the coating and substrate. The coating with high thermal expansion coefficient easily cracks under strong thermal stress. The thermal expansion coefficient disparity between the coating and substrate can cause the peeling from the substrate. The thermal expansion coefficient of  $\text{TiO}_2$  and  $\text{Ti6Al4V}$  is  $9 \times 10^{-6}$  and  $8.6 \times 10^{-6}$  m/K, respectively, whereas that of  $\text{Al}_2\text{TiO}_5$  is about  $1.5 \times 10^{-6}$  m/K [18]. The thermal shock test shows that the TMP coating spalls more severely than TMPAl, which is attributed to the higher thermal expansion coefficient of  $\text{TiO}_2$  compared to that of  $\text{AlTiO}_5$ . Although a large gap in thermal expansion coefficient exists

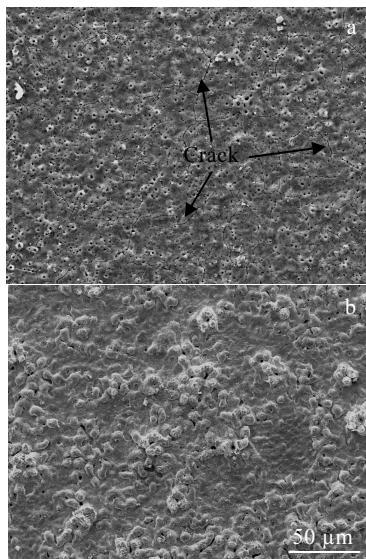


Fig.6 Surface SEM morphologies of the TMP (a) and TMPAl (b) coatings after oxidation at 700 °C for 100 h

**Table 3 Fitting oxidation kinetic equations of the Ti6Al4V substrate and TMP and TMPAl coating samples**

Sample	$n$	$k_p$	$D/\times 10^{-4}$	Equation
Ti6Al4V	1.48	0.21	1.55	$\Delta W^{1.48} = 0.21t$
TMP	1.01	0.0082	5.71	$\Delta W^{1.01} = 0.0082t$
TMPAl	1.95	0.0075	48	$\Delta W^{1.95} = 0.0075t$

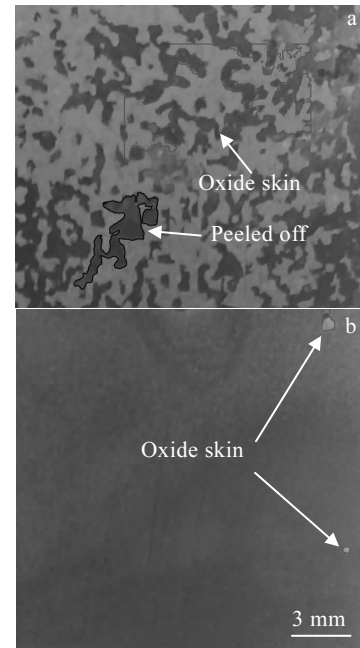


Fig.7 Digital images of the coating samples after thermal shock testing at 850 °C for 30 cycles: (a) TMP and (b) TMPAl

between  $\text{Al}_2\text{TiO}_5$  and  $\text{Ti6Al4V}$ , the metallurgical bond between the coating and substrate can be protected from spalling. Moreover, during the coating preparation process, the current of TMP is higher than that of TMPAl. Stronger and larger micro-arc discharges are also created in the former than in the latter. Greater stress is generated in the process of repeated calcination, which magnifies the thermal stress and causes the cracking and spalling off of the coating.

## 3 Conclusions

1) By adding  $\text{Al}_2\text{O}_3$  particles to the electrolyte, the  $\text{Al}_2\text{O}_3$  particles are sucked into the coating during the micro-arc oxidation process, which has a great influence on the roughness and denseness of the coating. The current density decreases during micro-arc oxidation with the addition of  $\text{Al}_2\text{O}_3$  particles.

2)  $\text{Al}_2\text{O}_3$  and  $\text{Al}_2\text{TiO}_5$  phases are combined in the slightly porous structure to provide good anti-oxidation effects at 700 °C for a long time.

3) The low coefficient of thermal expansion of  $\text{Al}_2\text{TiO}_5$  plays a crucial role in the anti-thermal-shock property of the coating at 850 °C.

## References

- Shen Yizhou, Tao Haijun, Lin Yuebin et al. *Rare Metal Materials and Engineering*[J], 2017, 46(1): 23
- Xue Wenbin, Wang Chao, Chen Ruyi et al. *Materials Let-*

- ters[J], 2002, 52(6): 435
- 3 Curran J A, Clyne T W. *Surface and Coatings Technology*[J], 2005, 199(2): 168
- 4 Tsunekawa S, Aoki Y, Habazaki H. *Surface and Coatings Technology*[J], 2011, 205(19): 4732
- 5 Yerokhin A L, Nie X, Leyland A et al. *Surface and Coatings Technology*[J], 2000, 130(2): 195
- 6 Wheeler J M, Collier C A, Paillard J M et al. *Surface and Coatings Technology*[J], 2010, 204(21): 3399
- 7 Habazaki H, Tsunekawa S, Tsuji E et al. *Applied Surface Science*[J], 2012, 259: 711
- 8 Li X, Han Y. *Applied Surface Science*[J], 2008, 254(20): 6350
- 9 Wang Yaming, Lei Tingquan, Jiang Bailing et al. *Applied Surface Science*[J], 2004, 233(1): 258
- 10 Tang H, Sun Q, Xin T et al. *Current Applied Physics*[J], 2012, 12(1): 284
- 11 Xu Y, Yao Z, Jia F et al. *Current Applied Physics*[J], 2010, 10(2): 698
- 12 Yao Z, Hu B, Shen Q et al. *Surface and Coatings Technology*[J], 2014, 253: 166
- 13 Li H, Sun Y, Zhang J. *Applied Surface Science*[J], 2015, 342: 183
- 14 Matykina E, Berkani A, Skeldon P et al. *Electrochimica Acta*[J], 2007, 53(4): 1987
- 15 Robinson H J, Markaki A E, Collier C A et al. *Journal of the Mechanical Behavior of Biomedical Materials*[J], 2011, 4(8): 2103
- 16 Wang Y, Jiang B, Lei T et al. *Materials Letters*[J], 2004, 58(12): 1907
- 17 Zhong Y, Shi L, Li M et al. *Applied Surface Science*[J], 2014, 311: 158
- 18 Kim I J, Supkwak H. *Canadian Metallurgical Quarterly*[J], 2014, 39(4): 387
- 19 Himmel L, Mehl R F, Birchenall C E, *JOM*[J], 1953, 5(6): 827

## Ti6Al4V 钛合金表面 Al<sub>2</sub>O<sub>3</sub> 颗粒改性微弧氧化涂层制备及性能

李 洪<sup>1</sup>, 宋智辉<sup>1,2</sup>, 唐 鹏<sup>1</sup>

(1. 广东省新材料研究所 现代材料表面工程技术国家工程实验室 广东省现代表面工程技术重点实验室, 广东 广州 510650)

(2. 广东工业大学, 广东 广州 510006)

**摘 要:** 通过在磷酸盐电解液中加入 Al<sub>2</sub>O<sub>3</sub> 陶瓷颗粒, 使得在 Ti6Al4V 钛合金表面的微弧氧化涂层结构和性能得到改性。涂层的结构和性能通过扫描电镜和 XRD 进行表征和测试, 涂层的抗高温氧化性能和热震性能通过高温热循环氧化试验和热震试验进行测试。结果表明, 通过在电解液中添加 Al<sub>2</sub>O<sub>3</sub> 陶瓷颗粒, 涂层由 Al<sub>2</sub>TiO<sub>5</sub> 和 TiO<sub>2</sub> 组成, 涂层更为致密, 表现出更为优异的抗高温氧化和热震性能。电解液中游动的 Al<sub>2</sub>O<sub>3</sub> 陶瓷颗粒在微弧氧化过程中被吸入到样品表面并进入涂层, 涂层的结构和性能得到改性。

**关键词:** Ti6Al4V 钛合金; 微弧氧化; Al<sub>2</sub>O<sub>3</sub> 颗粒; 抗氧化性能; 热震性能

**作者简介:** 李 洪, 男, 1987 年生, 博士, 广东省新材料研究所, 现代材料表面工程技术国家工程实验室, 广东省现代表面工程技术重点实验室, 广东 广州 510650, 电话: 020-37238071, E-mail: leehongaaaron@163.com